

MOLECULAR MECHANISM OF REVERSED TEMPERATURE DEPENDENCE OF ATP SYNTHESIS IN
GLACIER ICE WORMS

BY

NOUREEN ABDELRAHMAN

A thesis submitted to the

Graduate School-Camden

Rutgers, The State University of New Jersey

In partial fulfillment of the requirements

For the degree of Master of Science

Graduate Program in Computational and Integrative Biology

Written under the direction of

Dr. Grace Brannigan

And approved by

Dr. Grace Brannigan

Dr. Anthony Geneva

Dr. Daniel Shain

Camden, New Jersey
May 2023

THESIS ABSTRACT

MOLECULAR MECHANISM OF REVERSED TEMPERATURE DEPENDENCE OF ATP
SYNTHESIS IN GLACIER ICE WORMS

by Noureen Abdelrahman

Thesis Director:

Dr. Grace Brannigan

The F_0F_1 ATP synthase enzyme is highly conserved across species. The F_0F_1 is a reversible motor, where the counterclockwise rotation of the rotor portion of F_0 (known as the c-ring and present in the membrane-embedded F_0 domain) produces ATP, and the clockwise rotation induces ATP hydrolysis. In a surprising contrast to temperate organisms, glacier ice worms display elevated ATP levels as temperatures decline. The increased energy expenditure is used as a strategy for survival at cold temperatures, but the mechanism is unknown. More specifically, an ice worm-specific, 18 amino acid extension with regularly spaced histidine residues was previously found to be fused to the carboxy-terminal of the ATP6 subunit generating a proton shuttling domain projecting away from the F_0 exit pore. The role of this C-terminal extension in the temperature dependence ATP synthesis in ice worms is undetermined. To investigate the underlying mechanism of elevated ATP levels in glacier ice worms, we sought to understand the effects of temperature on the dynamics of the F_0F_1 ATP synthase of ice worm, yeast and ice worm without the ATP6 extension. We conducted all-atomistic MD simulations of the F_0 domain subunits at different temperatures to evaluate the effect of sequence on temperature dependence. We also measured the rotational diffusion of the c-ring as a function of temperature to evaluate the change in the rotation angles of the c-ring around the z-axis in clock-and counter-clockwise directions. Our results suggest that the rotational diffusion of the c-ring is temperature-dependent, and the ATP6 extension exacerbates the difference in rotational diffusion at varying temperatures.

ACKNOWLEDGMENTS

I would like to first acknowledge my mentor and PI: Dr. Grace Brannigan, who, through a lot of patience, guidance, and effort, has brought me up to my current scientific level. I am immensely grateful for everything that I have learned and continue to learn from Dr. Brannigan. I would also like to thank Drs. Anthony Geneva, Guillaume Lamoureux, and Daniel Shain for their advice and support on my project.

A special thank you goes to my lab mates and friends Connor, Ezry, Jahmal, and Jesse for mentoring and helping me in my scientific training. Their empathy, care, and support have kept me motivated, and they continue to make my time in the lab quite enjoyable.

Lastly, I want to thank my friends and family here and in Egypt, whose support and faith in me helped me get to where I am today. Thank you for always rooting for me!

DEDICATION

To my parents, Dalia and Aly. I would not have been here without your efforts and sacrifices.
Thank you for believing in me.

Table of Contents

Abstract	ii
Acknowledgements	iii
Dedication	iv
List of Figures	vi
1 Introduction	1
1.1 Glacier Ice worms	1
1.2 ATP Synthase in Eukaryotes: Structure and Function	1
1.3 Ice Worm ATP6 Extension	3
1.4 Molecular Dynamics Simulations: Challenges and Achievements	3
1.5 Research Approach	4
2 Methods	5
2.1 Multiple Sequence Alignment	5
2.2 Homology Modeling	5
2.3 MD Simulation Setup	6
2.4 Simulation Details	6
2.5 Trajectory Analyses	7
3 Results and Discussion	10
3.1 ATP6 Conservation Scores	10
3.2 ATP6 Flexibility	10
3.3 Rotational Diffusion of the c-ring	12
3.4 ATP6 Extension Orientation At Different Temperatures	15
4 Conclusions	16
Appendices	22

List of Figures

1.1	Mitochondrial F_1F_0 ATP Synthase Structure	2
2.1	Multiple Sequence Alignment of the ATP6 subunit	6
2.2	Predicted Structure of the F_0 ATP synthase structure of Ice Worm	7
2.3	RMSD analysis of the ice worm c-ring simulation trajectories at 310 K	9
3.1	ATP6 residues colored by conservation scores	10
3.2	ATP6 residues colored by the RMSF values for each sequence at each temperature .	11
3.3	Rotational Angles at 277 K and 310 K for each protein sequence	13
3.4	Temperature and Sequence dependence of rotational diffusion	13
3.5	Rotational Diffusion Constants for each system	14
3.6	Temperature-dependent interactions of the ATP6 extension with the protein	15
1	Correlation Relationship between the Conservation Scores and RMSF values	25

1 Introduction

1.1 Glacier Ice worms

The glacier ice worm, *Mesenchytraeus solifugus*, is one of the few metazoan species that completes its entire life cycle in freezing temperatures, close to 0 °C [1, 2]. Most freeze-tolerant/avoidant invertebrates are known to survive in temperatures that are well below 0 °C, but unlike glacier ice worms, they require several months of temperate climate each year to complete their life cycle. [3, 4]. Despite the metabolic constraints given by its cold habitat, the glacier ice worm activity level at 0 °C is comparable with its mesophilic counterparts (e.g. earthworm) at 10 °C and 20 °C. [5, 6]. Previous studies have also shown that, compared to temperate organisms, glacier ice worms display elevated adenosine triphosphate (ATP) levels at declining temperatures [7]. This unique energetic profile has been interpreted as a compensatory mechanism for adaptation in glacier ice, where the rate of ATP production in ice worms is significantly higher than the rate of ATP consumption, thus leading to higher ATP levels in ice worms than in their temperate counterparts [8].

1.2 ATP Synthase in Eukaryotes: Structure and Function

In eukaryotic organisms, the main source of ATP production is F_0F_1 ATP synthase, which synthesizes ATP in the mitochondrial matrix [9, 10]. F_0F_1 ATP synthases are part of a larger rotor protein family that also includes V- and A-type ATPases [11, 12]. The various ATPases are classified based on their function and taxonomic origin, but share a common structure and mechanism [13]. In addition to ATP synthesis, F-type ATPases can hydrolyze ATP and they are the primary source of ATP in the mitochondria, chloroplasts and bacterial plasma membrane. V-type ATPases are primarily found in eukaryotic vacuoles and they only hydrolyze ATP [12]. While F- and V-ATPases are both present in eukaryotes, the A-type ATPases are found solely in archaea. A-ATPases are evolutionarily more similar to V-ATPases [12] and they do both ATP production and ATP hydrolysis, like the F-ATPases [12]. A- and V-ATPases each have two and three peripheral stalks comprised of an E-G heterodimer, compared to the single peripheral stalk found in F-type ATP synthases [12, 14].

The F_0F_1 ATP synthase consists of two conjoined motors, F_1 , which lies in the mitochondrial matrix, and F_0 , which lies in the inner mitochondrial membrane (Figure 1.1). The F_1 domain is shaped like a mushroom head. It consists of three catalytic β subunits, three noncatalytic α subunits and the γ , δ , and ϵ subunits that constitute the central stalk, that connects the F_1 and F_0 domains [15] (Figure 1.1). The F_0 domain consists of the c-ring, which consists of 8-17 identical subunits, depending on the species [16], and subunit a (also known as ATP6 because it is encoded by the

ATP6 gene[16]), which lies adjacent to the c-ring. The peripheral stalk, which is located on one side of the complex, is made up of structural subunits *b*, *d*, *F6*, and *OSCP*[15].

The F_0F_1 is a reversible machine where ATP can be hydrolyzed in an F_1 domain connected to an F_0 domain working as a proton pump [17, 18]. This causes the central stalk of F_1 to rotate in the opposite direction and in turn the c-ring rotates in a clockwise direction (looking down at the cytoplasmic surface) during ATP hydrolysis.

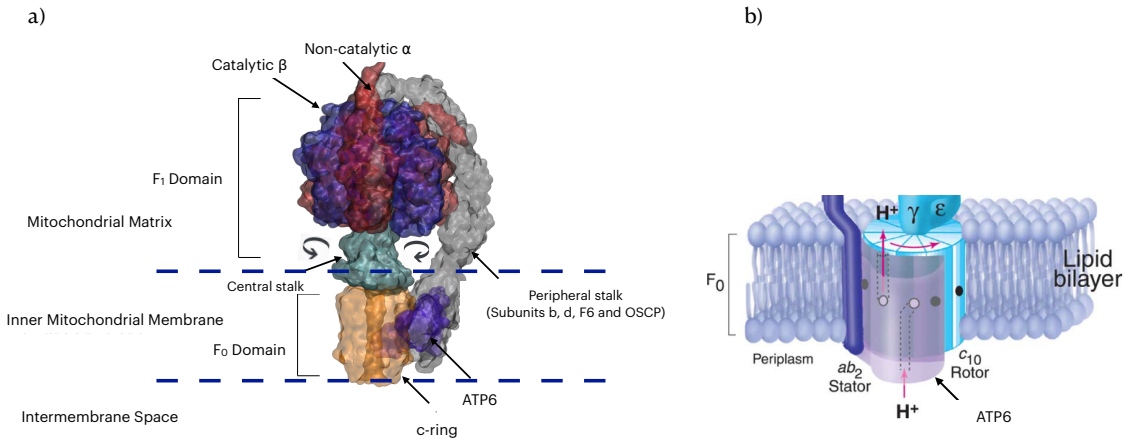


Figure 1.1: Mitochondrial F_0F_1 ATP Synthase Structure. a) Rotor–stator subunit structure in the mitochondrial F_1F_0 -ATP synthase: rotating c-ring subunits (orange), ATP6 (purple), three catalytic beta subunits (blue), three non-catalytic alpha subunits (red), central stalk (cyan) and the peripheral stalk (grey). The arrows indicate the reversible rotation that takes place during ATP synthesis (“counterclockwise” or left direction, looking down at the cytoplasmic surface) and hydrolysis (“clockwise” or right direction, looking down at the cytoplasmic surface). b) Protons enter the mitochondrial membrane through the periplasmic proton entry channel and bind to Asp-61 (open circle). The protonated binding site (filled circle) then moves towards the lipid (hydrophobic) phase of the membrane where it reaches the exit channel on the cytoplasmic side (mitochondrial matrix) of the membrane to release the proton. The γ and ϵ subunits are fixed on top of one set of c subunits, so that the c-ring rotation drives rotation of subunit γ (central stalk). Figure 1.1b is reprinted with permission from [19].

ATP is synthesized from ADP and inorganic phosphate (Pi) in the F_1 domain. This process is driven by a proton motive force, where protons flow down a concentration gradient from the intermembrane space to the inner mitochondrial membrane [14, 20]. ATP6 consists of two integral, hydrophilic, half-channels that act as the proton entry and exit sites (Figure 1.1b). As the H^+ ions flow into the mitochondrial membrane through the proton entry channel, they bind to the Asp-61 residue of the c-ring causing its protonation into Aspartic acid. That triggers the rotation of the

c-ring, in a counterclockwise direction (looking down at the cytoplasmic surface), which allows the hydrophobic Aspartic acid to face inwards towards the core of the protein [19, 20]. When the c-ring undergoes a counterclockwise rotation, one of its multiple Asp/Glu residues comes closest to the Arg(+) of subunit a, causing its deprotonation. The proton is then released via the half channel facing the mitochondrial matrix (Figure 1.1b) [18, 21]. The protonation/deprotonation of the c-ring residues drives the rotation of the c-ring. Each c-ring subunit has one binding site for a membrane-crossing ion, and translocates one H⁺ ion per revolution. Therefore, the ratio of ions per ATP is theoretically determined by the stoichiometry of the c-ring [2, 10]. The counterclockwise rotation (looking down at the cytoplasmic surface) of the c-ring generates a torque that triggers the movement of the central stalk, thus causing conformational changes in the mushroom head of the F₁ domain, favoring the uphill process of ATP synthesis within its catalytic subunits [18].

1.3 Ice Worm ATP6 Extension

A broad genomics survey of the F₀F₁ ATP synthase of ice worms has shown a striking modification in the C-terminus of ATP6 in ice worms [22]. Specifically, a Histidine-rich region of 18 amino acids has been observed. Histidine is an ionizable amino acid and exists both in neutral and protonated forms in the body, which allows it to be both acid and base at physiologic pH. This unique property makes Histidine a quick proton shuttle. It can do this by extracting a proton with its basic nitrogen to make a positively charged intermediate and then uses another buffer molecule to extract the proton from its acidic nitrogen [23]. Therefore, it is hypothesized that the Histidine-rich ATP6 extension in ice worms could be used to accelerate the rate of proton flow across the membrane [7]. In this work, we focus solely on the F₀ domain of the F₀F₁ ATP synthase to investigate the role of the ATP6 extension in temperature-dependent ATP synthesis. We use the amino acid sequences from ice worms that were collected in the American Pacific Northwest by Daniel Shain and his coworkers.

1.4 Molecular Dynamics Simulations: Challenges and Achievements

In the past few decades, atomistic simulation methods have made enormous strides toward understanding the structure-function interactions of biomolecules [24]. Millisecond-long simulations of small molecules and peptides are now possible thanks to substantial advancements in hardware design, distributed computing techniques, and effective sampling procedures [18]. Yet, when examining cellular processes that entail huge macromolecules operating through tightly connected chemical and mechanical events, a significant hurdle is encountered. For a very large system, simulating the macromolecule at the atomistic level (i.e., by modeling every atom of the molecule along

with water, ions, and/or membrane) often requires enormous processing resources [24]. This challenge is exacerbated by the fact that small time scale simulations, for bigger macromolecules, fall short of defining the mechano-chemical (or rotary-chemical) action of molecular motors. Short time scale simulations yield atomistic trajectories in the range of a few hundred nanoseconds (or few microseconds), and as a result, they can only accurately represent the system's local dynamics. This is insufficient to explain the kinetic and thermodynamic principles of the entire molecular motor, whose mechanical events take place over a wide range of timescale, which extends beyond the millisecond regime [24].

There have been numerous attempts to use atomistic or coarse-grained (CG) molecular dynamics simulations to study the behavior of the F_1 [25–29] and F_0 [30] motors. These studies have uncovered intriguing structural information about the fundamental chemical and mechanical states of the F_0 and F_1 motors. In addition, some research have resorted to applying external forces (or torques) to accommodate the structural changes necessary for the motor action in order to get around the challenge of replicating lengthy time scale processes [25, 29]. While those attempts have made it possible to comprehend how the 3D structure of the F_0F_1 motor dynamically adapts to huge forces that are absent from real biological systems, they haven't yet fully revealed the structure-based energetics of the mechano-chemical interaction [18]. To our knowledge, there haven't been any investigations into the effect of temperature on the energetics of the F_0F_1 motor.

1.5 Research Approach

The ATP6 subunit is attached to the c-ring at the proton exit site. This suggests that the change in the c-ring rotational diffusion, as a function of temperature, can affect the ATP6 conformation, which likely affects the rate of ATP production. We hypothesize that the poorly conserved residues of ATP6 will experience the most fluctuations in simulations. To test that hypothesis, we calculated the conservation scores of the ATP6 residues to identify the highly and poorly conserved residues. Then, we calculated the RMSF of ATP6 to measure the fluctuations of the residues under both temperatures. We are particularly interested in the ice worm ATP6 extension. Therefore, we predicted the structure of the ice worm F_0 domain using homology modeling. To investigate the underlying mechanism of elevated ATP levels in glacier ice worms and evaluate the effect of sequence on temperature dependence, we conducted all-atomistic MD simulations of the F_0 domain of the ice worm, ice worm without the ATP6 extension and yeast (control) at low (277 K) and high (310 K) temperatures. We also measured the rotational diffusion of the c-ring as a function of temperature to evaluate the change in the rotation angles of the c-ring around the z-axis.

2 Methods

2.1 Multiple Sequence Alignment

Multiple Sequence Alignments (MSA) and conservation scores were calculated using UGENE Unipro (Figure 2.1) [31]. Conservation scores are calculated by dividing the number of different amino acids at a given site by the frequency of the most common amino acid at that site [32]. The complete alignments can be found in Appendix 1.

2.2 Homology Modeling

To generate a predicted structure for the F_0 domain of the ice worm (Figure 2.2), Modeller [33] was used. To construct a model, all comparative modeling algorithms rely on a set of assumed structural equivalences between the target and template residues based on the alignment of the target and template sequences [34]. The ice worm sequences for each subunit were aligned against the respective yeast sequence using MEGA software [35]. The yeast F_0 protein sequences (PDB ID: 6CP7) were used as the template sequences and the aligned ice worm F_0 protein sequences as target sequences. To obtain better quality loops for the predicted structure, the LoopModel class in Modeller was used. The structures, that were generated by Modeller, were then loaded into MolProbity [36] to add and fully optimize all the hydrogen atoms, both polar and nonpolar [37].

To assess the stability of the predicted ice worm structure in simulation, the root mean square deviation (RMSD) of the c-ring simulation trajectories was plotted using the *RMSD Trajectory Tool* in VMD (Figure 2.3). RMSD is a measure of how much the atomic positions of the particles deviated from a reference position at t=0 ns during the simulation. It is calculated for MD simulation trajectories to assess the stability of the simulated system. Figure 2.3 shows that the ice worm strucutre reached thermal equilibration/stability at about 225 ns.

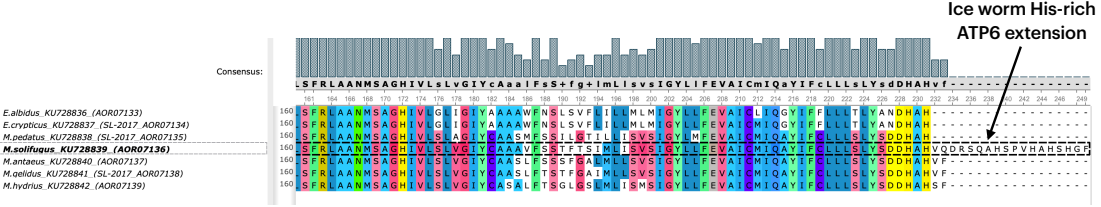


Figure 2.1: **Multiple Sequence Alignment of the ATP6 subunit.** Multiple Sequence Alignment of the ATP6 of worm species belonging to the *Enchytraeus* and *Mesenchrytaeus* genera, using Ugene Unipro. *M. solifugus* (ice worm) has the longest amino acid sequence, owing to the histidine-rich 18-amino acid extension. The most common amino acids are colored at each column. (See full alignment in Appendix 1).

2.3 MD Simulation Setup

All F_0 domains were embedded in a POPC bilayer membrane using CHARMM-GUI Membrane Builder [38]. For yeast, a cryoEM structure for the yeast F_0 ATP Synthase (PDB ID: 6CP7) was used. The protein was oriented along the z-axis, normal to the membrane, and the water thickness (minimum height on the top and bottom of the system) was 12.0 angstroms. The POPC bilayer was built using 320 phosphatidylcholine (POPC) molecules (about 160 in each leaflet). A total of 98 Na⁺ and 139 Cl⁻ ions were randomly placed by CHARMM-GUI to neutralize the system and provide a salt concentration of 0.15 M NaCl. The system was approximately 120, 120, and 125 angstroms in x, y, and z dimensions, respectively, with about 170000 total atoms that included 36271 TIP3P waters. The previous workflow was repeated using the ice worm and ice worm without ATP6 extension predicted structures.

2.4 Simulation Details

Atomistic molecular dynamics simulations were run on the yeast, ice worm and ice worm without ATP6 extension structures at 277 K and 310 K using NAMD v2.14 [39]. The CHARMM36 [38] model was used for the protein, phospholipids, TIP3P waters and ions parameters. All six simulations (yeast at 277 K and 310 K, ice worm at 277 K and 310 K, ice worm without ATP6 extension at 277 K and 310 K) used periodic boundary conditions and particle mesh Ewald (PME) electrostatics. Interactions between non-bonded atoms were cut off at 12 Å, and bonds involving hydrogen were

constrained using the SHAKE/RATTLE algorithms. A Langevin thermostat and barostat were used to maintain a temperature and pressure of either 277 K or 310 K and 1 atm, respectively. The time step for each simulation was 2 fs. Prior to production, the restraints were gradually lowered to aid in the system equilibration, and 100 minimization steps were required.

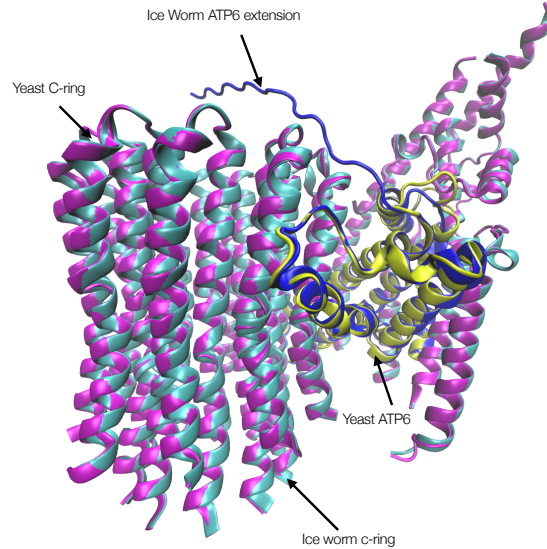


Figure 2.2: Predicted Structure of the F_0 ATP synthase structure of Ice Worm. Ice worm F_0 aligned on Yeast F_0 , where cyan represents the ice worm structure, with ATP6 colored in blue, and magenta represents the yeast structure, with ATP6 colored in yellow.

2.5 Trajectory Analyses

All trajectories were visualized using the Visual Molecular Dynamics (VMD) software [40]. The trajectories were aligned to the backbone of the protein structure before measuring the following: Root-mean-square fluctuation (RMSF) of ATP6 and the rotational angle of the c-ring around the z axis. The RMSF was measured for residue alpha carbons and describes the fluctuation of each residue relative to the average position of the residue over all time steps in each simulation. The RMSF of the ATP6 residues was calculated using the *measure rmsf* command in VMD. This command returns the root mean square position fluctuation for each selected atom in the selected frames, using the following equation:

$$\rho_i^{RMSF} = \sqrt{\langle (r_i - \langle r_i \rangle)^2 \rangle} \quad (2.1)$$

where ρ_i^{RMSF} is the RMSF of residue i, r_i is the reference position of the alpha carbon of residue i, $\langle r_i \rangle$ is the average position of residue i over all timesteps and $\langle (r_i - \langle r_i \rangle)^2 \rangle$ is the square root of the

variance of the position.

Correlation Analysis was then performed between the conservation scores (section 2.1) and calculated RMSF values (Equation 2.1). The correlation analysis is performed by calculating the R-squared value of the linear fit. The R-squared value measures the proportion of variation in the dependent variable (y-axis) that can be attributed to the independent variable (x-axis) and is calculated using the following equation:

$$R^2 = 1 - \frac{\text{sum squared regression (SSR)}}{\text{total sum of squares (SST)}} \quad (2.2)$$

where sum squared regression is the sum of the residuals squared, and the total sum of squares is the sum of the distance the data is away from the mean squared.

The rotational angle around the z axis (θ) was measured using the *spinAngle* component in the Collective Variables Dashboard (Colvars) in VMD [41]. The component *spinAngle* returns an angle (in degrees) within the periodic interval $[-180 : 180]$. The rotational angles were used to calculate the Mean Square Displacement (MSD) of the residues of the c-ring as a function of the timesteps, using the following random walk diffusion equation:

$$\langle x^2(t) \rangle = 2Dt \quad (2.3)$$

where x is the displacement (degrees), D is the rotational diffusion coefficient ($\text{degree}^2/\text{ns}$) and t is time (ns). The random walk equation above is used to describe the diffusion of particles in one dimension (in our case, that is the z dimension). To obtain the value of the diffusion coefficient D , the slope of the $\langle x^2(t) \rangle$ vs. Δt plot is calculated and divided by 2. To evaluate the variance in the rotational angles that were measured using Colvars, we calculated the standard error of the mean for the $\langle x^2 \rangle$ values using the following equation:

$$SEM = \frac{\sigma}{\sqrt{n}} \quad (2.4)$$

where σ is the standard deviation of the rotational angles across timesteps, and n is the sample size of the squared average rotational angles values of the linear fit.

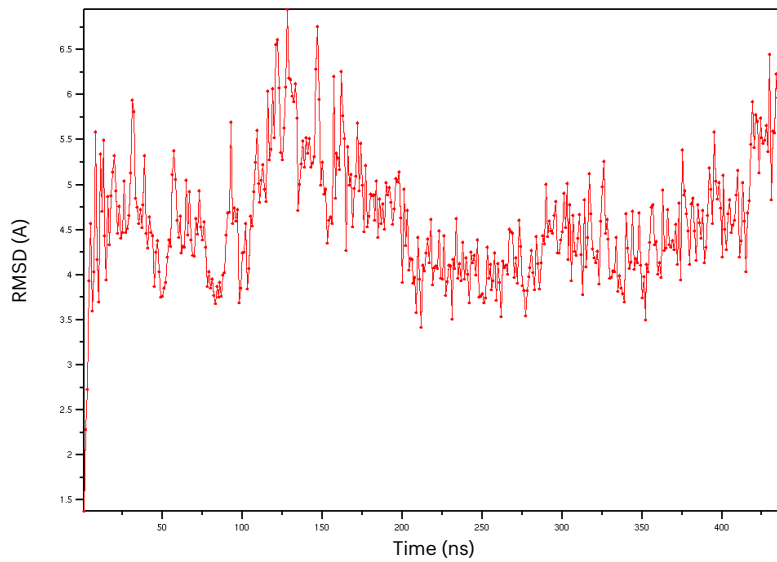


Figure 2.3: RMSD analysis of the ice worm c-ring simulation trajectories at 310 K, using only the backbone atoms of the c-ring subunits for alignment. Simulation time of ~ 400 ns shows that the predicted structure of the ice worm F_0 domain gets equilibrated (stabilized) during the course of simulation with respect to reference frame at time 0 ns.

3 Results and Discussion

3.1 ATP6 Conservation Scores

Conservation Scores of ATP6 residues were calculated from the Multiple Sequence Alignment of worms belonging to the *Enchytraeus* and *Mesenchytraeus* genera (Figure 2.1). The conservation scores showed that the the ATP6 subunit is highly conserved, with the C-terminus being more poorly conserved than the rest of the subunit regions (Figure 3.1). Past studies have shown that both termini of the ATP6 subunit are poorly conserved, and that the poorly conserved regions of ATP6 do not seem critical for proton translocation [42, 43].

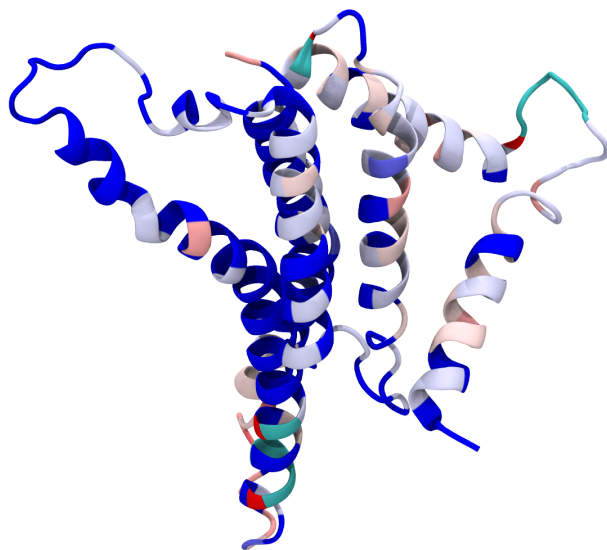


Figure 3.1: ATP6 residues colored by conservation scores from the MSA of worm species belonging to the *Enchytraeus* and *Mesenchytraeus* genera. The ATP6 Subunit (cartoon structure) is colored by conservation. The conservation scores range from 29% (dark red) as the most poorly conserved to 100% (dark blue) as the most highly conserved. Conservation scores were determined via multiple sequence alignment of ATP6 sequences from homologous worm sequences (Section 2.1).

3.2 ATP6 Flexibility

To understand the flexibility of ATP6 at different temperatures, we calculated the RMSF of ATP6 for the ice worm, yeast and ice worm without ATP6 extension structures at 277 K and 310 K. In Figure 3.2, the ATP6 (cartoon structure) of the a) yeast, b) ice worm, and c) ice worm without APT6 extension is colored by the RMSF values at both temperatures: 277 K and 310 K. A high RMSF value for any given residue indicates greater flexibility because the atom has significantly deviated from its reference position. In Figure 3.2b, the ice worm ATP6 extension at 277 K has

significantly higher RMSF values than the rest of the subunit, indicating its instability and high fluctuations in simulations compared to the other ATP6 residues. Moreover, we observed higher RMSF values of the ATP6 extension at 277 K than at 310 K, which shows that the ATP6 extension is more dynamic at low temperatures. We performed a correlation analysis between the ATP6 RMSF values and conservation scores. The correlation analysis for all six systems produced a coefficient of determination (R-squared value) of less than 0.3, meaning that, contrary to our hypothesis, there is no correlation between the ATP6 conservation scores and RMSF values (see results of correlation analysis in Appendix 2).

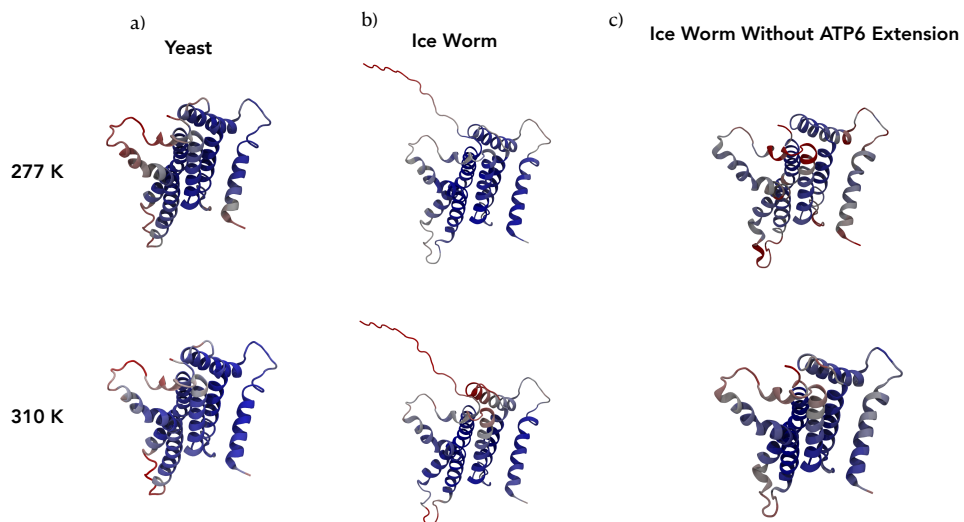


Figure 3.2: ATP6 residues colored by the RMSF values for each sequence at each temperature. The ATP6 Subunit (cartoon structure) lies in the membrane-embedded F_0 domain of the F_1F_0 ATP Synthase complex (grey). ATP6 is colored by RMSF values. The RMSF values range from 0.73 (dark blue) to 6.31 (dark red) as the least to most fluctuations, respectively, across all systems except b) the ice worm at 277 K. The RMSF values of the ATP6 extension residues in the ice worm at 277 K range from 11 to 19, while the rest of the ATP6 residues range from 0.65 to 4.15.

3.3 Rotational Diffusion of the c-ring

To measure the rotational diffusion coefficient of the c-ring, we measured the rotational angle of the c-ring around the z-axis (θ), for each system, in clock-and counter-clockwise directions. The net rotational and average rotational angles for each simulation system is shown in Figure 3.3. Figure 3.3a shows the net rotation in each simulation system and how much the structure adjusted from $t=0$ ns until it equilibrated. After equilibration (~ 250 ns), the system is stabilized and the rotation is observed as thermal fluctuations around a small range of angles. In Figure 3.3b, there is a shift in the average rotational angle of yeast (control sequence), where the average rotational angle increases when cooled down. The difference between the average rotational angles of yeast at 277 K and that at 310 K is statistically significant ($p < 10^{-10}$). The same trend is observed in the ice worm sequence between the average rotational angles at 277 K and 310 K. These results indicate that the rotational angle of the c-ring is more stable as the Temperature increases. However, the opposite behavior is observed in the ice worm without ATP6 extension sequence, where the rotational angle is less stable with increasing temperature. The difference between the average rotational angles at 277 K and 310 K is also statistically significant ($p < 10^{-10}$). The rotational angles, of the equilibrated timesteps, were used to calculate the mean square displacement of the c-ring at different timesteps, for each temperature (Figure 3.4).

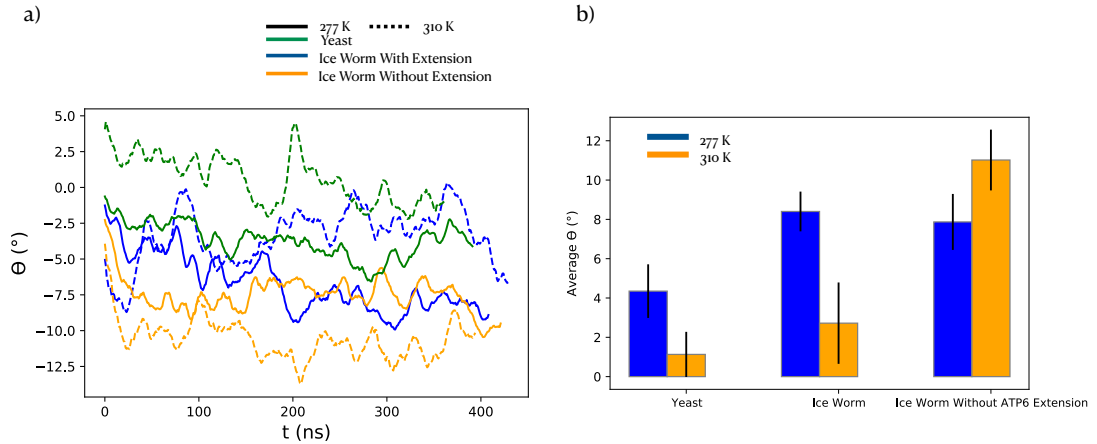


Figure 3.3: **Rotational Angles at 277 K and 310 K for each protein sequence.** a)The dashed lines represent simulations at 310 K, and the solid lines represent simulations at 277 K. The simulations all start at a specific rotational angle (θ) (section 2.5) then fluctuate significantly until they equilibrate. After equilibration, the simulations fluctuate over a small range of angles due to stabilization. b) The blue bars represent the average rotational angles (θ) at 277 K, whereas the orange bars represent the average rotational angles at 310 K. The average rotational angle (θ) varies between sequences based on how long each simulation system took to reach thermal equilibration (i.e. the amount of time it took to bring the system to the desired temperature and pressure conditions). Error bars were calculated from the standard deviation of the rotational angle (θ) values at each interval for 400 ns.

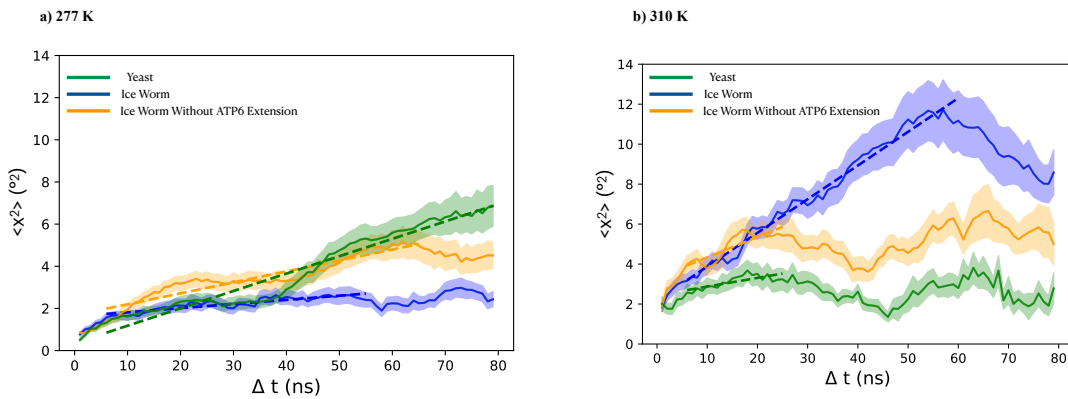


Figure 3.4: **Temperature and Sequence dependence of rotational diffusion.** MSD of the yeast ATP synthase c-ring rotation around the z-axis as a function of t (Equation 2.3) from a NAMD simulation over ~ 150 ns at a) 277K and b) 310 K. The dashed lines represent a linear fit to Equation 2.3, and correspond to diffusional displacement.

Then, we calculated the rotational diffusion coefficient (D) and observed that the yeast, ice worm, and ice worm without the ATP6 extension systems all have a faster rotational diffusion coefficient at 310 K than at 277 K (Figures 3.4 and 3.5). This indicates that the rotational diffusion of the c-ring of the F_0F_1 ATP synthase is indeed temperature-dependent, as expected. However, the temperature-dependent difference in diffusion varies per sequence (Figure 3.5). In Figure 3.5, we see that the change in Temperature does not affect the rotational diffusion of the yeast significantly, whereas it has a big effect on the ice worm and ice worm without ATP6 extension sequences. The ratio between the rotational diffusion coefficient of yeast at 277 K to that at 310 K is 0.9, which is very high compared to a ratio of 0.1 in the ice worm, and a ratio of 0.4 in the ice worm without ATP6 extension. This suggests that the ATP6 extension exacerbates the temperature sensitivity of the protein. The difference between the average rotational diffusion coefficients of the ice worm and ice worm without ATP6 extension at 277 K is statistically significant ($p < 10^{-10}$), indicating that the ATP6 extension does indeed lower the rotational diffusion of the c-ring.

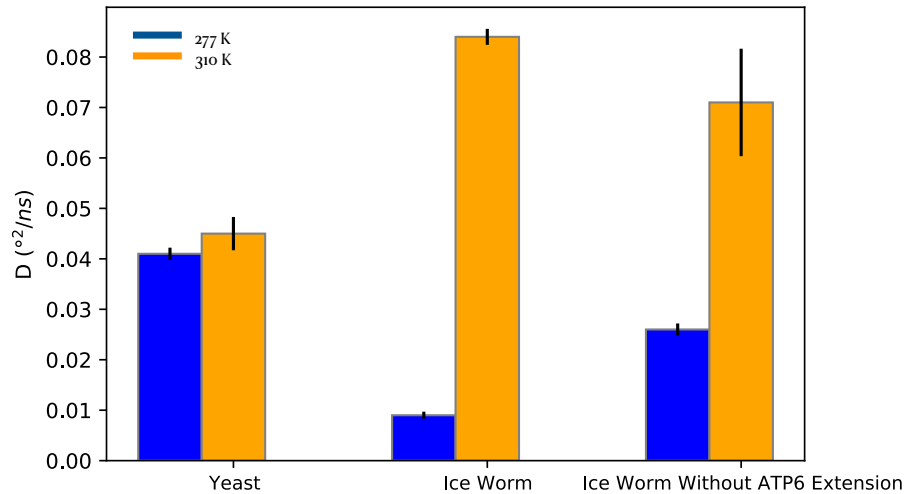


Figure 3.5: Rotational Diffusion Constants for each system at 277 K and 310 K. The blue bars represent the rotational diffusion constants at 277 K, whereas the orange bars represent the rotational diffusion constants at 310 K (Equation 2.3 and Figure 3.4). The error bars were calculated using the standard error values of the fitted line on the MSD plot (Equation 2.4 and Figure 3.4).

3.4 ATP6 Extension Orientation At Different Temperatures

In our simulations of the ice worm systems at 277 K and 310 K, we observed different behavior for the ATP6 extension at each temperature. At 277 K, the ATP6 extension flipped back at ~10 ns and bound to a structural chain (subunit *b*) (Figure 3.6a). For the remainder of the simulation time (~400 ns), the extension unbound and bound back again twice, then it remained bound to subunit *b* (Multiple Sequence Alignment of subunit *b* can be found in Appendix 1 C). At 310 K, a different behavior was observed: the ATP6 extension did not flip back. Instead, it partially inserted itself in the c-ring lumen (Figure 3.6b). We do not think that is realistic behavior since in the real-life model of F_0F_1 ATP synthase, the central stalk acts as a cap on top of the c-ring (Figure 1.1), which would prevent the ATP6 extension from inserting itself into the c-ring lumen. These results suggest that there are favorable interactions between the ATP6 extension and subunit *b* at 277 K, that are unstable at 310 K. Since high temperatures favor the entropy factor, it is possible that the binding of the ATP6 extension to subunit *b* is an entropically unfavorable process, therefore it was not observed at 310 K.



Figure 3.6: Temperature-dependent interactions of the ATP6 extension with the protein. a) Ice Worm simulation over ~400 ns at 277 K. The ATP6 extension is colored by Timestep, where it starts facing left at 0 ns, then proceeds to flip back at ~10 ns, until it flips all the way back and binds to subunit *b* (frontview). b) Ice Worm simulation over ~400 ns at 310 K. The ATP6 extension does not flip back. It partially inserts itself into the c-ring lumen (topview).

4 Conclusions

In this work, we investigated an MT-ATP6 extension mutation that is present in ice worms [6, 7]. We ran simulations using yeast, ice worm and ice worm without the ATP6 extension sequences at 277 K and 310 K. We found that the rotational diffusion of the F_0 c-ring is temperature-dependent, with a faster diffusion at 310 K. The difference in diffusion between 277 K and 310 K varied for each sequence. However, a large statistically significant difference in rotational diffusion constants was observed in the ice worm, compared to the ice worm without ATP6 extension. This shows that the ATP6 extension has a role in increasing the temperature sensitivity of the protein. It remains unclear to us whether a lower or higher c-ring diffusion is more efficient for ATP production, however based on our results, we hypothesize that a lower c-ring rotational diffusion increases the efficiency of ATP production in the membrane.

We also found that at 277 K, the ice worm ATP6 extension binds to subunit *b*, that connects the F_0 and F_1 domains, a behavior that was not found in the ice worm system at 310 K. That behavior could be due to the thermodynamic fact that high temperatures favor the entropy factor. It is possible that the binding of the ATP6 extension to subunit *b* affects the rate of proton flow outside of the membrane, however, since only one replica was run of each simulation, there aren't enough data to make that claim about the behavior of the ATP6 extension.

Bibliography

- [1] Angela H. Farrell, Kristi A. Hohenstein, and Daniel H. Shain. Molecular Adaptation in the Ice Worm, *Mesenchytraeus solifugus*: Divergence of Energetic-Associated Genes. *Journal of Molecular Evolution*, 59(5):666–673, nov 2004.
- [2] Alexander Hahn, Kristian Parey, Maike Bublitz, Deryck J. Mills, Volker Zickermann, Janet Vonck, Werner Kühlbrandt, and Thomas Meier. Structure of a Complete ATP Synthase Dimer Reveals the Molecular Basis of Inner Mitochondrial Membrane Morphology. *Molecular Cell*, 63(3):445–456, aug 2016.
- [3] L. Sømme and T. Birkemoe. Cold tolerance and dehydration in Enchytraeidae from Svalbard. *Journal of Comparative Physiology B: Biochemical, Systemic, and Environmental Physiology*, 167(4):264–269, may 1997.
- [4] P. G. Pedersen and M. Holmstrup. Freeze or dehydrate: only two options for the survival of subzero temperatures in the arctic enchytraeid *Fridericia ratzeli*. *Journal of Comparative Physiology B: Biochemical, Systemic, and Environmental Physiology*, 173(7):601–609, sep 2003.
- [5] D. Goodman. Ecological Investigations Of Ice Worms on Casement Glacier, Southeastern Alaska. Institute of Polar Studies Report No. 39. *Office of Scientific and Technical Information (OSTI)*, jan.
- [6] Daniel H. Shain, Tarin A. Mason, Angela H. Farrell, and Lisa A. Michalewicz. Distribution and behavior of ice worms (*Mesenchytraeus solifugus*) in south-central Alaska. *Canadian Journal of Zoology*, 79(10):1813–1821, oct 2001.
- [7] Shirley A. Lang and Daniel H. Shain. Atypical Evolution of the F1Fo Adenosine Triphosphate Synthase Regulatory ATP6 subunit in Glacier Ice Worms (Annelida: Clitellata: Mesenchytraeus). *Evolutionary Bioinformatics*, 14:117693431878807, jan 2018.
- [8] Shirley A. Lang, Patrick McIlroy, and Daniel H. Shain. Structural Evolution of the Glacier Ice Worm Fo ATP Synthase Complex. *The Protein Journal*, 39(2):152–159, feb 2020.
- [9] Massimo Bonora, Simone Patergnani, Alessandro Rimessi, Elena De Marchi, Jan M. Suski, Angela Bononi, Carlotta Giorgi, Saverio Marchi, Sonia Missiroli, Federica Poletti, Mariusz R. Wieckowski, and Paolo Pinton. ATP synthesis and storage. *Purinergic Signalling*, 8(3):343–357, apr 2012.

- [10] Jasmine A. Nirody, Itay Budin, and Padmini Rangamani. ATP synthase: Evolution, energetics, and membrane interactions. *Journal of General Physiology*, 152(11), sep 2020.
- [11] Richard L. Cross and Volker Müller. The evolution of A-, F-, and V-type ATP synthases and ATPases: reversals in function and changes in the H⁺-ATP coupling ratio. *FEBS Letters*, 576(1-2):1–4, sep 2004.
- [12] L. K. Lee, A. G. Stewart, M. Donohoe, R. A. Bernal, and D. Stock. Crystal structure of the peripheral stalk of *Thermus thermophilus* H+-ATPase/synthase. *Nature Structural and Molecular Biology*.
- [13] Masashi Toei, Regina Saum, and Michael Forgac. Regulation and Isoform Function of the V-ATPases. *Biochemistry*, 49(23):4715–4723, may 2010.
- [14] An I. Jonckheere, Jan A. M. Smeitink, and Richard J. T. Rodenburg. Mitochondrial ATP synthase: architecture, function and pathology. *Journal of Inherited Metabolic Disease*, 35(2):211–225, aug 2012.
- [15] John E. Walker. ATP Synthesis by Rotary Catalysis (Nobel lecture). *Angewandte Chemie International Edition*, 37(17):2308–2319, sep 1998.
- [16] T. Meier, P. Polzer, K. Diederichs, W. Welte, and P. Dimroth. *Science*.
- [17] Wolfgang Junge and Nathan Nelson. ATP Synthase. *Annual Review of Biochemistry*, 84:631–657, 2015.
- [18] Shayantani Mukherjee and Arieh Warshel. The FOF1 ATP synthase: from atomistic three-dimensional structure to the rotary-chemical function. *Photosynthesis Research*, 134(1):1–15, jul 2017.
- [19] Robert H. Fillingame, Christine M. Angevine, and Oleg Y. Dmitriev. Mechanics of coupling proton movements to c-ring rotation in ATP synthase. *FEBS Letters*, 555(1):29–34, oct 2003.
- [20] Paul D. Boyer. THE ATP SYNTHASE: A Splendid Molecular Machine. *Annual Review of Biochemistry*, 66(1):717–749, jun 1997.
- [21] Wolfgang Junge. ATP Synthase: Electro-Chemical Transducer with Stepping Rotatory Mechanics. In *Photosynthesis: Mechanisms and Effects*, pages 1635–1642. Springer Netherlands, 1998.

- [22] Marie T. Lott, Jeremy N. Leipzig, Olga Derbeneva, H. Michael Xie, Dimitra Chalkia, Mahdi Sarmady, Vincent Procaccio, and Douglas C. Wallace. mtDNA Variation and Analysis Using Mitomap and Mitomaster. *Current Protocols in Bioinformatics*, 44(1), dec 2013.
- [23] Zoë Fisher, Jose A. Hernandez Prada, Chingkuang Tu, David Duda, Craig Yoshioka, Haiqian An, Lakshmanan Govindasamy, David N. Silverman, and Robert McKenna. Structural and Kinetic Characterization of Active-Site Histidine as a Proton Shuttle in Catalysis by Human Carbonic Anhydrase II. *Biochemistry*, 44(4):1097–1105, jan 2005.
- [24] Arieh Warshel. ChemInform Abstract: Multiscale Modeling of Biological Functions: From Enzymes to Molecular Machines (Nobel Lecture). *Angewandte Chemie International*, 45:no–no, 2014.
- [25] Rainer A. Böckmann and Helmut Grubmüller. Nanoseconds molecular dynamics simulation of primary mechanical energy transfer steps in F1-ATP synthase. *Nature Structural and Molecular Biology*.
- [26] Jacek Czub and Helmut Grubmüller. Torsional elasticity and energetics of F1-ATPase. *Proceedings of the National Academy of Sciences*, 108(18):7408–7413, apr 2011.
- [27] Kwangho Nam, Jingzhi Pu, and Martin Karplus. Trapping the ATP binding state leads to a detailed understanding of the F1-ATPase mechanism. *Proceedings of the National Academy of Sciences*, 111(50):17851–17856, dec 2014.
- [28] Kei ichi Okazaki and Gerhard Hummer. Phosphate release coupled to rotary motion of F1-ATPase. *Proceedings of the National Academy of Sciences*, 110(41):16468–16473, sep 2013.
- [29] Jingzhi Pu and Martin Karplus. How subunit coupling produces the -subunit rotary motion in F1-ATPase. *Proceedings of the National Academy of Sciences*, 105(4):1192–1197, jan 2008.
- [30] D. Pogoryelov, A. Krah, J. Langer, O. Yildiz, J. D. Faraldo-Gomez, and T. Meier. Microscopic rotary mechanism of ion translocation in the Fo complex of ATP synthases. *Nature Chemical Biology*, oct 2010.
- [31] Konstantin Okonechnikov, Olga Golosova, and Mikhail Fursov. Unipro UGENE: a unified bioinformatics toolkit. *Bioinformatics*, 28(8):1166–1167, feb 2012.
- [32] Fredrik Johansson and Hiroyuki Toh. A comparative study of conservation and variation scores. *BMC Bioinformatics*, 11(1), jul 2010.

- [33] Andrej Šali and Tom L. Blundell. Comparative Protein Modelling by Satisfaction of Spatial Restraints. *Journal of Molecular Biology*, 234(3):779–815, dec 1993.
- [34] András Fiser and Andrej Šali. Modeller: Generation and Refinement of Homology-Based Protein Structure Models. In *Methods in Enzymology*, pages 461–491. Elsevier, 2003.
- [35] Koichiro Tamura, Glen Stecher, and Sudhir Kumar. MEGA11: Molecular Evolutionary Genetics Analysis Version 11. *Molecular Biology and Evolution*, 38(7):3022–3027, apr 2022.
- [36] Christopher J. Williams, Jeffrey J. Headd, Nigel W. Moriarty, Michael G. Prisant, Lizbeth L. Videau, Lindsay N. Deis, Vishal Verma, Daniel A. Keedy, Bradley J. Hintze, Vincent B. Chen, Swati Jain, Steven M. Lewis, W. Bryan Arendall, Jack Snoeyink, Paul D. Adams, Simon C. Lovell, Jane S. Richardson, and David C. Richardson. MolProbity: More and better reference data for improved all-atom structure validation. *Protein Science*, 27(1):293–315, nov 2018.
- [37] I. W. Davis, A. Leaver-Fay, V. B. Chen, J. N. Block, G. J. Kapral, X. Wang, L. W. Murray, W. B. Arendall, J. Snoeyink, J. S. Richardson, and D. C. Richardson. MolProbity: all-atom contacts and structure validation for proteins and nucleic acids. *Nucleic Acids Research*, 35(Web Server):W375–W383, may 2007.
- [38] Sunhwan Jo, Taehoon Kim, Vidyashankara G. Iyer, and Wonpil Im. CHARMM-GUI: A web-based graphical user interface for CHARMM. *Journal of Computational Chemistry*, 29(11):1859–1865, mar 2008.
- [39] Julio D. C. Maia John E. Stone Joao V. Ribeiro Rafael C. Bernardi Ronak Buch Giacomo Fiorin Jerome Henin Wei Jiang Ryan McGreevy Marcelo C. R. Melo Brian K. Radak Robert D. Skeel Abhishek Singharoy Yi Wang Benoit Roux Aleksei Aksimentiev Zaida Luthey-Schulten Laxmikant V. Kale Klaus Schulten Christophe Chipot James C. Phillips, David J. Hardy and Emad Tajkhorshid. Scalable molecular dynamics on CPU and GPU architectures with NAMD. *Journal of Chemical Physics*, 2020.
- [40] 18-Humphrey W.; Dalke A.; Schulten K. VMD: Visual Molecular Dynamics. *J. Mol. Graph.*, 1997.
- [41] Giacomo Fiorin, Michael L. Klein, and Jérôme Hénin. Using collective variables to drive molecular dynamics simulations. *Molecular Physics*, 111(22-23):3345–3362, dec 2013.

- [42] Soledad Funes, Edgar Davidson, M. Gonzalo Claros, Robert van Lis, Xochitl Pérez-Martinez, Miriam Vázquez-Acevedo, Michael P. King, and Diego González-Halphen. The Typically Mitochondrial DNA-encoded ATP6 Subunit of the F1F0-ATPase Is Encoded by a Nuclear Gene in Chlamydomonas reinhardtii. *Journal of Biological Chemistry*, 277(8):6051–6058, feb 2002.
- [43] Gunjan Katyal, Brad Ebanks, Magnus Lucassen, Chiara Papetti, and Lisa Chakrabarti. Sequence and structure comparison of atp synthase f0 subunits 6 and 8 in notothenioid fish. *PLOS One*, jan 2021.

Appendices

Appendix 1 A: ATP6 Multiple Sequence Alignment of Worm Species Belonging to the *Enchytraeus* and *Mesenchytraeus* genera

E.albidus_KU728836_(AOR07133)	MMPDIFSSFDPPSSFSNIIIPSMТИMFMINIYMFIDRNWMSMEANRTVLSLPILQSMVPEVERTYMFNIN	70
E.crypticus_KU728837_(SL-2017_AOR07134)	MMPDIFSSFDPPSSFSNIIIPSMТИMFMINIYMFIDRNWMSMETNRTVLSLPILQSMVPEVERTYMFNIN	70
M.pedatus_KU728838_(SL-2017_AOR07135)	MMPDIFSSFDPPFMNTLAPSNSMFTLINVNLILLM0QSFWIMNSOKSALMNEITQOLIFTQLSRNTVHFK	70
M.solifugus_KU728839_(AOR07136)	MMPDIFSSFDPPFMNSVPSNSIIFLCINVNLLILSM0QSFWIMGSRKSSFMNEIVQVIFSQSLSRTVHLK	70
M.antaeus_KU728840_(AOR07137)	MMPDIFSSFDPPFMNTLVPNSNIFLCINVNMLILM0QSFWIIGSOKSSFMNEIVQLIFTQLSRNTVHFK	70
M.gelidus_KU728841_(SL-2017_AOR07138)	MMPDIFSSFDPPFMNTLVPNSNIFLCINVNMLILM0QSFWIIGSOKSSFMNEIVQLIFTQLSRNTVHFK	70
M.hydrus_KU728842_(AOR07139)	MMPDIFSSFDPPFMNSVPSNSVFLCINNILLM0QSFWIIGSRKSAFMNEIVQLIFTQLSRNTVHFK	70
***** *:: ** :::: *:: : :: .. * : :::: : * * : ::::* .. :		
E.albidus_KU728836_(AOR07133)	PLNQLMHQIFFMVIVLNLMGLFPYTFSTSISHLHFTLISIGLPMWMLLIIMSSAIKSIKATIAHLLPEGAPDW	140
E.crypticus_KU728837_(SL-2017_AOR07134)	PLNQLMHQIFFMVIVLNLMGLFPYTFSTSISHLHFTLISIGLPMWMLLIIMSSAIKSIKATIAHLLPEGAPDW	140
M.pedatus_KU728838_(SL-2017_AOR07135)	GLSSLVSSIFVTILNLLGPIPYMFSTSSHLLFTLTIGLPWVLMSVLSFTSKFVASVAHFLPDGAPDW	140
M.solifugus_KU728839_(AOR07136)	GLSSLVSSIFVTILNLLGPIPYMFSTSSHLLFTLTIGLPWVLMSVLSFTSKFVASVAHFLPDGAPDW	140
M.antaeus_KU728840_(AOR07137)	GLSSLVSSIFVTILNLLGPIPYMFSTSSHLLFTLTIGLPWVLMSVLSFTSKFVASVAHFLPDGAPDW	140
M.gelidus_KU728841_(SL-2017_AOR07138)	GLSSLVSSIFVTILNLLGPIPYMFSTSSHLLFTLTIGLPWVLMSVLSFTSKFVASVAHFLPDGAPDW	140
M.hydrus_KU728842_(AOR07139)	GLSSLVSSIFVTILNLLGPIPYMFSTSSHLLFTLTIGLPWVLMSVLSFTSKFVASVAHFLPDGAPDW	140
*.:: *. ::::*;*:: ** ::::*;*::*;*::*;*::*;*::*;*::*;*::*;*::*;*::*;*::*;		
E.albidus_KU728836_(AOR07133)	LNPFLVLIIESSSIIVPRITLFSRLAAMNSAGHIVLGLIGIYAAAAWFNSLSVFLILLMLMIGYLLFEVAI	210
E.crypticus_KU728837_(SL-2017_AOR07134)	LNPFLVLIIESSSIIVPRITLFSRLAAMNSAGHIVLGLIGIYAAAAWFNSLSVFLILLMLMIGYLLFEVAI	210
M.pedatus_KU728838_(SL-2017_AOR07135)	LNPFLVLIETTSISVPRPLTSFRLAAMNSAGHIVLGLAGIYCAASMFSSILGTILLISVSIGYLFEVAI	210
M.solifugus_KU728839_(AOR07136)	LNPFLVLIETTSISVPRPLTSFRLAAMNSAGHIVLGLIGIYCAAFFSFTSISLMLISVSIGYLFEVAI	210
M.antaeus_KU728840_(AOR07137)	LNPFLVLIETTSISVPRPLTSFRLAAMNSAGHIVLGLIGIYCAASLFTGAIMLLSVSIGYLFEVAI	210
M.gelidus_KU728841_(SL-2017_AOR07138)	LNPFLVLIETTSISVPRPLTSFRLAAMNSAGHIVLGLIGIYCAASLFTGAIMLLSVSIGYLFEVAI	210
M.hydrus_KU728842_(AOR07139)	LNPFLVLIETTSISVPRPLTSFRLAAMNSAGHIVLGLIGIYCASALFTGAIMLLSVSIGYLFEVAI	210
***** *:: ***;*::*;*::*;*::*;*::*;*::*;*::*;*::*;*::*;*::*;		
E.albidus_KU728836_(AOR07133)	CLIQGYIFFLLTLYANDHAH-----	249
E.crypticus_KU728837_(SL-2017_AOR07134)	CMIQAYIFFLLTLYANDHAH-----	249
M.pedatus_KU728838_(SL-2017_AOR07135)	CMIQAYIFCLLSSLYSDDDHAH-----	249
M.solifugus_KU728839_(AOR07136)	CMIQAYIFCLLSSLYSDDHQDRSQAHSVPVAHSHGF	249
M.antaeus_KU728840_(AOR07137)	CMIQAYIFCLLSSLYSDDHAHVF-----	249
M.gelidus_KU728841_(SL-2017_AOR07138)	CMIQAYIFCLLSSLYSDDHAHVF-----	249
M.hydrus_KU728842_(AOR07139)	CMIQAYIFCLLSSLYSDDHHSF-----	249
::.*::*;*::*;*::*;*::*;		

Appendix 1 B: ATP6 Pairwise Sequence Alignment of Ice Worm versus Rotifer

```

rotifer_ATP6 -----MTLGFSVVMLMLLFMNFS---LGSNKINMVS--VYNIFMDIKVISVYLVK 70
ice_worm_ATP6 MMPDISSFDPPMFNSVPSNSIFLCINVLLILSMQSSFWMGRKSSFMNEIVQVIFSQLSRTSTVHLK 70
                           :: :: : *::* *: *   :**.* .:. * ** :.. *. :*
rotifer_ATP6 FMSAVVFLFLNYNSYIYYSGVVTMSYGYVFIYALSMVLVWLWSVNMIN---MVSFLPLGIEGI 140
ice_worm_ATP6 GLSSLVSSIFVAIILINLFGLIPYMFSTSSHLLIFTLTIGLPWLSMVMSFTKSFKASVAHFLPDGAPDW 140
                           :*: :* :*: .. : * . :*: :* : * :*: .. : *:**** * .
rotifer_ATP6 LKTFIPILELIGVLIRPLTLAIRLATNISCGHVVLLMF-----SFFAFNVANYLVMSISLLLFGLYFIE 210
ice_worm_ATP6 LNPFLVLIETTSIMVRPLTLSFRLAANMSAGHIVSLVGIVCAAASFSTFTSIMLISVSI---GYLLFE 210
                           *:.*: :*: .:::*****:***;*:.*:*** :.   ..*: ..: .:::***: * :*
rotifer_ATP6 FLVCMIQAYVFWSLIYIYMMMDMEI----- 252
ice_worm_ATP6 VAICMIQAYIFCLLSSLYSDDHAHVQDRSQAHSPVHAHSHGF 252
                           . :*****: * :* :* *

```

Appendix 1 C: Subunit *b* Multiple Sequence Alignment

Appendix 2: Correlation Analysis between ATP6 RMSF values and Conservation Scores

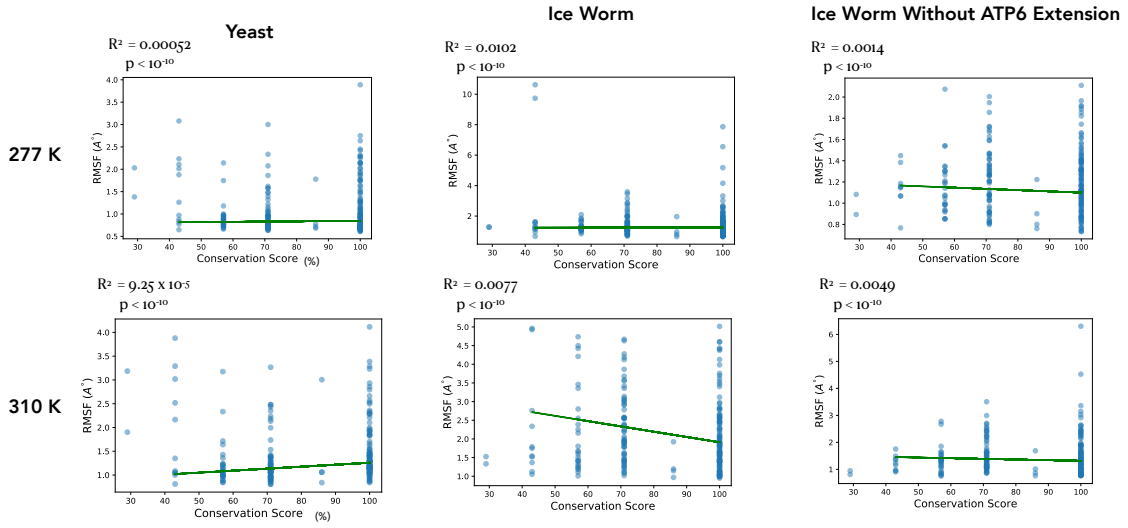


Figure 1: Correlation Relationship between the Conservation Scores and RMSF values. Plots of the RMSF values per residue (Equation 2.1, Section 2.5) for each system vs. the Conservation Scores of each residue (Section 2.1). The green line in each plot represents a linear fit. The R^2 values (Equation 2.2) of all six systems are < 0.3 which indicates that the independent variable (Conservation Score) does not explain the variation of the dependent variable (RMSF). A horizontal linear fit means no correlation between the conservation scores and RMSF values. The p-values of all six systems are less than 10^{-10} indicating no statistical significance.